Effect of Torrefaction on Aerosol Emissions at Combustion Temperatures Relevant for Domestic Burning and Power Generation

Charles Perrie[a], Chase K. Glenn[a], Gregory Reed[b], Tret C. Burdette[c], Khairallah Atwi[a], Omar El Hajj[a], Zezhen Cheng[a,†], Kruthika V. Kumar[a], Amanda A. Frossard[c], Sudhagar Mani[b], and Rawad Saleh[a*].

[a] Air Quality and Climate Research Laboratory, School of Environmental, Civil, Agricultural and Mechanical Engineering, University of Georgia, Athens, GA 30602, USA

[b] School of Chemical, Materials, and Biological Engineering, University of Georgia, Athens, GA 30602, USA

[c] Department of Chemistry, University of Georgia, Athens, GA 30602, USA

ABSTRACT: Torrefied biomass is a promising carbon-neutral alternative for coal. However, the effect of torrefaction on aerosol production in biomass combustion is understudied. Here, we compared the emissions and physicochemical properties of aerosols produced by the combustion of raw pine, torrefied pine, and bituminous coal. At the highest combustion temperature of 1000 °C, aerosol emissions from coal were 5.2 ± 0.4 mg/MJ, while emissions from raw and torrefied pine were negligible (< 10^{-2} mg/MJ). The coal-combustion aerosol was dominated by inorganics (85%) with a small organic fraction (15%), a composition typical of condensable particulate matter observed in power-generation applications. At the lowest combustion temperature of 400 °C, aerosol emissions from raw pine (25.3 ± 4 mg/MJ) and torrefied pine (5.6 ± 0.8 mg/MJ) were dominated by organics. The organic molecules probed using electrospray ionization mass spectrometry were dominated by CHO and CHNO groups for both raw and torrefied pine. Torrefied-pine emissions featured less aromatics (17% vs 22%), which can be attributed to the reduction in volatile-matter content associated with torrefaction. Overall, our findings support the adoption of torrefied pine for domestic burning and power generation because of the added benefit of reducing aerosol emissions in addition to being carbon-neutral.

Synopsis statement: In addition to being carbon-neutral, torrefied biomass has the added benefit of reducing particulate emissions in domestic and industrial applications.

Keywords: Biomass, coal, combustion, particulate matter, electrospray ionization mass spectrometry.

Introduction

Coal and biomass are widely used solid fuels throughout the world [1]. They account for over 200 exajoules of energy annually [2,3], approximately one-third of the total global energy consumption[2,4]. Both fuels are used in industrial and residential settings. Over 3 billion people use coal and biomass for residential heating and cooking[1,5], and despite efforts to phase out coal from power plants, it still accounts for 36% of the global power production[3].

Biomass is one of the viable renewable (carbon-neutral) alternatives to coal, either by replacement or co-firing in power plants[6]. In 2020, the European Union set a target for 55% reduction in greenhouse gas emissions by 2030, with utilizing biomass playing a major role in the proposed plan. While biomass is widely available from multiple sources including agriculture (corn stalks, cotton, cotton bush, surplus food), waste (vine and tree pruning, food waste, forest residue), and harvested trees[7–10], there are major limitations associated with using biomass in place of or in conjunction with coal. First, biomass has a significantly lower carbon content compared to coal, thus a lower heating value (energy density)[11]. Second, the moisture content of biomass can inhibit efficient combustion[12–14]. Third, biomass in its raw form is difficult to transport, store, and feed it into existing gasification and combustion systems[15,16]. These limitations can be largely overcome by thermally treating the biomass in a process called torrefaction [17–19]. By heating the biomass to temperatures ranging between 200°C and 300°C, the fibrous structure and the tenacity of the biomass are destroyed[20], and oxygen and water are removed via

carboxylation and dehydration, respectively[8,19]. This brings the torrefied biomass heating values closer to that of coal[11].

Torrefied biomass has been explored as an option to complement or replace coal[9,11,21]. A recent techno-economic analysis suggested that torrefied biomass can be produced at a competitive market price compared to conventional raw biomass, and can be comparable to coal if carbon credits are included in the analysis[22]. While replacing coal with biomass, including torrefied biomass, has a climate benefit due to the reduction in greenhouse gas emissions, the impact on emissions of air pollutants, including aerosols (or particulate matter, PM), is less clear. The combustion of both coal and biomass produces high concentrations of aerosol emissions, especially in low-efficiency domestic burning[23–26], but also in industrial processes[27,28]. Due to their significant public-health impacts[29,30], emissions from domestic cookstoves have been extensively studied. Aerosol – specifically PM with sizes smaller than 2.5 μm ($PM_{2.5}$) – emission factors from cookstoves reported in the literature range over 3 order of magnitude from 10^{-1} g/kg-fuel to 10^{2} g/kg-fuel [31–33]. With biomass and coal having heating values on the order of 10^{1} MJ/kg [11,17], the range of emission factors per unit energy translates to 10^{-2} g/MJ – 10^{1} g/MJ. This wide variation is attributed to several factors including differences in fuels, cookstove type, and operation conditions[34–38]. Aerosol emissions from solid fuel combustion in power generation applications are typically lower than domestic burning[33], which is expected given the more complete combustion in those applications.

There is an important distinction in aerosol formation pathways between domestic and power-generation combustion. Aerosols emitted from domestic combustion are dominated by carbonaceous species, including elemental carbon (EC) and organic carbon (OC)[36,39,40]. On the other hand, due to the more complete combustion conditions in power-generation applications, the carbon in the fuel is more efficiently converted to CO_2. Under such conditions, the aerosol emissions are often dominated by inorganic species [28,41] and their formation potential is correlated with the ash content of the fuel[18]. Torrefied biomass fuels usually have higher ash content than their raw counterparts[42]. This has been hypothesized to lead to the higher aerosol mass emissions from the combustion of torrefied biomass compared to raw biomass observed in several studies at conditions representative of power-generation combustion [18,43]. Studies on domestic combustion of torrefied biomass are scarce. Maxwell et al.[44] burned three biomass fuels (willow, spruce, and olive stone) in raw and torrefied form in a domestic fixed-bed stove and showed that aerosol mass emissions from the torrefied fuels were lower than their raw counterparts. This was attributed to the reduction in volatile organic species – which have high sooting propensity (i.e. potential to form carbonaceous aerosol) – in the biomass associated with torrefaction.

In this study, we investigate the effect of torrefaction on the emission factors and physicochemical properties (size distributions, chemical composition, and light-absorption properties) of the aerosol emitted from the combustion of pine. Because biomass has been considered as an alternative to coal, we also compare the aerosol emissions from the combustion of raw and torrefied pine to those from the combustion of bituminous coal. In order to isolate the effect of fuel type, we performed controlled-combustion experiments that ensured consistent combustion conditions across fuels, thus leaving fuel type as the only variable. The experiments were performed at temperatures ranging between 400 °C and 1000 °C to capture conditions relevant for combustion in both domestic and power-generation settings.

Methods

Fuel preparation

The combustion experiments were performed using 3 fuels: (1) raw pine, (2) torrefied pine, and (3) bituminous coal. Pine chips were acquired from a saw mill operation in Oglethorpe Georgia and the bituminous coal was obtained from the Central Steam Plant at the University of Georgia. The torrefied pine was prepared in a batch reactor as described in Manouchehrinejad and Mani[17]. Briefly, the raw pine chips were heated in an electric furnace (Thermolyne Furnace, Type 30400, Dubuque, Iowa) at a rate of 3 °C/min to a torrefaction temperature of 275 °C under oxygen-free conditions that were maintained by flowing 2 L/min of nitrogen through the reactor. The pine chips were kept at 275 °C for 30 min. All fuels were ground using a heavy-duty knife mill (Retsch SM 2000, Germany). The resulting pulverized fuels were then separated using two sieves in series in order to isolate fuel particles with sizes between 90 μm and 120 μm for the combustion experiments.

Fuel properties were obtained as described in Manouchehrinejad and Mani[17] and Phanphanich and Mani[11], and are presented in Table 1. Proximate analysis of the fuels was performed using a micro thermo-gravimetric analyzer (TGA701, LECO Corporation, St. Joseph, MI) following ASTM D 7582 [45]. Ultimate analysis was performed using an elemental analyzer (LECO CHNS 932, LECO Corporation, St. Joseph, MI) following ASTM D3176 [46]. The higher heating value (HHV) of the fuels was obtained using an adiabatic oxygen bomb calorimeter (IKAC, 2000, IKA Works, Inc., NC) following ASTM D5865 [47].

Table 1. Fuel properties of raw pine, torrefied pine, and bituminous coal

Fuel	Moisture Content (%, wb)	Volatile Matter (%, db)	Ash (%, db)	Fixed Carbon (%, db)	C (%, db)	H (%, db)	N (%, db)	O (%, db)	HHV (MJ/kg)
Raw Pine	6.69 (0.11)	85.90 (0.01)	0.27 (0.02)	13.76 (0.02)	47.21 (0.28)	6.64 (0.01)	0.17 (0.05)	45.76 (0.53)	18.46 (0.13)
Torrefied Pine	2.46 (0.10)	76.40 (0.27)	0.35 (0.03)	23.26 (0.23)	54.91 (0.27)	6.20 (0.10)	0.2 (0.00)	38.17 (0.13)	21.82 (0.08)
Bituminous coal	1.57 (0.05)	36.58 (0.02)	6.52 (0.05)	56.91 (0.20)	77.63	6.3	2.00	9.16	27.72 (0.02)

Combustion experiments

A schematic of the experimental setup is shown in Figure 1. The combustion experiments were performed using a steady-flow reactor at an air-to-fuel ratio of 25 and at combustion temperatures of 400 °C, 600 °C, 800 °C, and 1000 °C. This temperature range was chosen to encompass the temperatures encountered at different stages in domestic combustion[48], and the higher temperatures (800 °C and 1000 °C) overlap with those in previous studies that simulated power-generation combustion conditions[28,43,49]. The fuel particles were supplied into a combustion reactor at a controlled mass flow rate, in a fashion similar to the drop-tube furnace or one-dimensional furnace configurations commonly employed in pulverized coal and biomass combustion studies[49–51]. We utilized a custom-built particle feeder system based on the design of Molinder and Wiinikka[52]. The particle-feeder system consists of a vertically mounted glass hopper attached to a syringe pump pusher block. A ¼" diameter stainless steel tube leads from the center of the glass hopper down into the combustion chamber. The syringe pump pushes the fuel hopper up at a set speed, allowing the fuel particles to fall down the stainless-steel tube and into the combustion chamber along with clean carrier air introduced at the top of the hopper. The carrier air was supplied by a house compressor and was passed through a filter train comprised of a silica gel denuder, and activated carbon denuder, and a HEPA filter. We maintained the carrier air flowrate at 1 L/min and the pumping speed of the syringe pump was adjusted to achieve the desired fuel mass flowrate to maintain an air-to-fuel ratio of 25. Two vibration motors were attached to the fuel hopper to agitate the fuel particles and prevent sticking on the walls of the hopper.

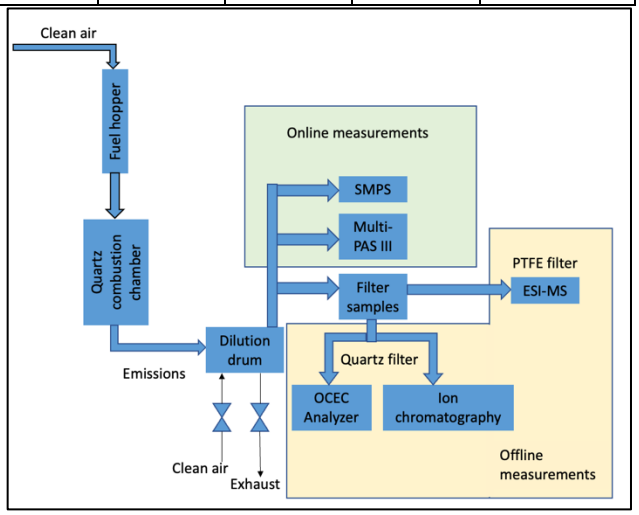

Figure 1. Schematic of the experimental setup.

The combustion chamber is a custom-built cylindrical quartz tube (~0.1 L) enclosed in a heating jacket. The power of the heating jacket was controlled using a proportional-integral-derivative (PID) controller to achieve the desired set temperature measured at the center of the combustion chamber using a high-temperature K-type thermocouple. With an air flow of 1 L/min, the average residence time in the combustion chamber was approximately 6 s. As shown in Figure 1, the combustion emissions were diluted using clean air in a 250 L drum to both lower the aerosol concentrations and dampen fluctuations for the online measurements. Dilution flowrates ranged between 16.5 and 38.7 L/min, leading to an average residence time in the dilution drum of 5.2 – 17.8 min.

As described in the previous subsection, the fuel particle sizes in our experiments ranged between 90 µm and 120 µm. This relatively narrow size distribution was chosen to ensure a stable feed rate into the combustion chamber. Furthermore, utilizing a narrow fuel particle size distribution minimizes variability in combustion conditions between experiments, such that differences in emissions between experiments can be attributed to fuel type, and not combustion conditions. We note that the fuel particle sizes employed in this study are consistent with pulverized coal and biomass particle sizes in power-generation applications (usually on the order of 10^1 µm – 10^2 µm)[53,54] and laboratory drop-tube furnace studies[31,55]. However, domestic burning applications usually do not utilize pulverized fuels. The relatively large sizes of biomass or coal (e.g. briquettes or

chunks) in domestic burning lead to complex combustion conditions dictated by heterogeneity in temperature and air-to-fuel ratio, which exhibit spatial and temporal variability[48]. While our controlled-combustion setup does not capture this complexity, it enables exploring well-constrained combustion conditions within the parameter space (temperature and air-to-fuel ratio). In this study, we focus on isolating the effect of temperature on aerosol emissions by performing the combustion experiment at different temperatures (400 °C – 1000 °C) that encompass those encountered in domestic combustion[48].

Online measurements

We measured the aerosol size distributions over the size range of 10 nm – 500 nm at a 90-second resolution using a scanning mobility particle sizer (SMPS, TSI). The SMPS consists of a differential mobility analyzer (DMA, TSI, Model 3081A00), an advanced aerosol neutralizer (TSI, Model 3088), and a condensation particle counter (CPC, TSI, Model 3772). The SMPS size distributions were integrated to obtain the total submicron aerosol mass concentration assuming a density of 1 g/cm^3. We also measured the absorption coefficients (b_{abs}) of the aerosol emissions at a 1-second resolution at 3 wavelengths that cover the visible spectrum (422 nm, 532 nm, and 782 nm) using a photoacoustic spectrophotometer (Multi-PAS III)[56]. Due to the low absorption signal at 782 nm, only measurements at 532 nm and 422 nm were used in the analysis described below.

We calculated the emission factors (EF) of 3 key parameters (aerosol mass, number of ultrafine aerosol particles, and aerosol absorption) per unit of fuel energy supplied. The emission factors were calculated as:

$$\mathrm{EF} = \frac{X \,.\, D \,.\, V_{air}}{m_{fuel} \,.\, \mathrm{HHV}} \qquad (1)$$

Where, D is the dilution factor in the dilution drum (Figure 1), V_{air} is the carrier air volumetric flow rate, m_{fuel} is the fuel mass flowrate, and HHV is the fuel higher heating value (Table 1). For aerosol mass emission factors (EF_{mass} [mg/MJ]), X in Equation (1) is the aerosol mass concentration obtained from integrating the SMPS mass distribution. For number emission factors of ultrafine particles (EF_{UF} [particles/MJ]), X is the number concentration of ultrafine particles obtained from integrating the SMPS number distribution for particles with diameters less than 100 nm. The aerosol absorption emission factors (EF_{abs} [m^2/MJ]) represent the total absorption cross-section of the emitted aerosol[57], where X is the absorption coefficient [1/m] obtained from the Multi-PAS III measurements.

We also performed optical closure analysis to retrieve the imaginary part of the refractive indices (k) of the aerosol [58–60]. This involved Mie calculations of absorption coefficients using SMPS size distributions and treating k as a free parameter to match calculated absorption coefficients with those measured using the Multi-PAS III. We assumed a wavelength-independent real part of the refractive index of 1.6 in the Mie calculations[61].

Saleh (2020)[62] classified light-absorbing organic aerosol, or brown carbon (BrC) into optical classes based on pairs of k at 550 nm (k_{550}) and wavelength dependence of k (w). For experiments that produced aerosol with measurable absorption at both 422 nm and 532 nm, we calculated w and k_{550} as:

$$w = \frac{\log(k_{532}/k_{422})}{\log(422/532)}\,,\; k_{550} = k_{532}\,(532/550)^{w} \qquad (2)$$

Where, k_{422} and k_{532} are k values at 422 nm and 532 nm, respectively. For reference, w is related to the absorption Ångström exponent (AAE), where in the small-particle limit, $w \approx \mathrm{AAE} - 1$.

Offline measurements

For select experiments, the aerosol emissions were collected on quartz (PALL Life Sciences, 47 mm) and polytetrafluoroethylene (PTFE) (SterliTech Corporation, 47 mm) filters for offline chemical analysis. We targeted a particle loading for approximately 300 µg on each filter.

The quartz filter was used to determine the fractions of organic carbon (OC), elemental carbon (EC), and major inorganic ions (K^+, Na^+, NH_4^+, Cl^-, SO_4^{2-}, and NO_3^-). A 1.5 cm^2 punch was taken from the filters for OC/EC analysis using an OCEC Analyzer (Sunset Laboratories, USA) following the NIOSH 870 protocol (A. Karanasiou & W. Maenhaut, 2015; Birch & Cary, 1996). The remainder of each Quartz filter was placed in pre-cleaned glass vial with 20 ml of ultra-pure water and sonicated for 10 minutes. Immediately after, 5 ml of the solution was analyzed for inorganic ions using Dionex Integrion high-pressure ion chromatography (IC) instruments (Thermo-Fischer, USA).

The PTFE filters were used to further investigate the chemical make-up of the organic aerosol fraction using ultra-high-resolution electrospray ionization mass spectrometry (ESI-MS). The aerosol particles were extracted from the filters in methanol following the procedure described in Cheng et al.[63]. Briefly, each filter was placed in a pre-cleaned glass vial with 3 ml methanol and sonicated for 10 minutes. The methanol solution was then filtered through a 13 mm PTFE syringe filter (0.2 µm) to remove any particles that were dislodged during sonication but not soluble in methanol. The methanol was evaporated to a final volume of approximately 1 ml to concentrate the solution. ESI-MS analysis was performed using a Brüker SolariX XR 12T Fourier-transform ion cyclotron resonance (FTICR) mass spectrometer in negative ionization mode over m/z range of 74 – 600. The ESI-MS mass spectra were analyzed using the open-source software MFAssignR (Schum et al., 2020). Prior to assignments, sample noise was calculated using built-in functions, and the mass spectra were filtered to obtain peaks with a S/N threshold ≥ 3. C^{13} and S^{34} isotopes were identified from a preliminary C, H, and O assignment set, and a list of species with these isotopes was created and checked to confirm molecular formulas. Final formulas were assigned with filters of N ≤ 3 and S ≤ 1. A blank PTFE filter, prepared using the same procedure as the samples, was used to filter out background peaks.

Results and Discussion

Emission factors

Figure 2a depicts the mass emission factors of the aerosols (EF_{mass}) emitted from the combustion of raw pine, torrefied pine, and coal at different combustion temperatures. Both raw

pine and torrefied pine exhibited an inverse relation between EF_{mass} and combustion temperature. This trend indicates that the combustion efficiency of these fuels increased with increasing temperature, thus reducing the emissions of partially oxidized species, including aerosols. An important practical implication of this finding is that utilizing these biomass fuels in power-generation applications, where the combustion temperatures are relatively high[28,43,49,64], is expected to produce low aerosol emissions. On the other hand, biomass combustion in domestic settings, where starting and burnout temperatures are relatively low, leads to high levels of aerosol emissions, as previously reported in various domestic-burning studies[34–37].

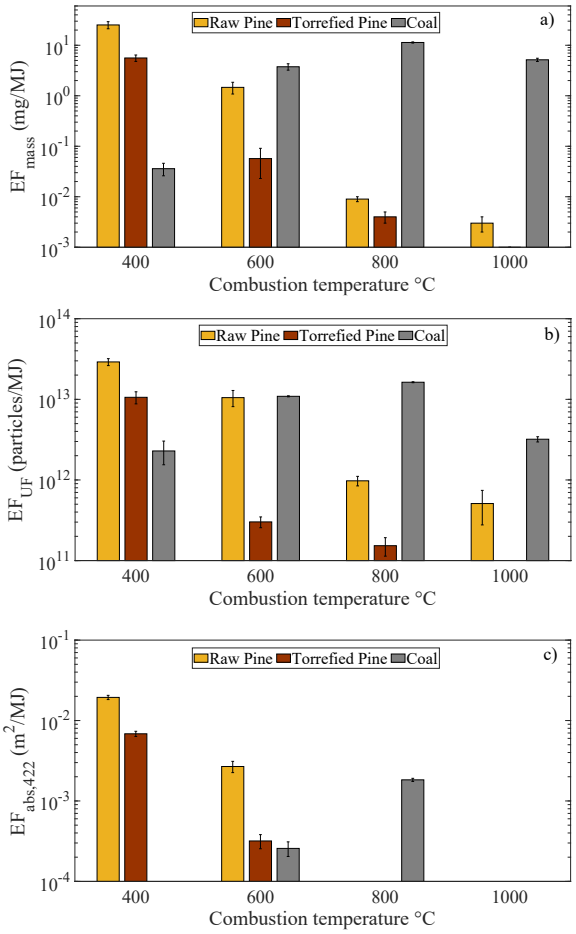

Figure 2. Emission factors at different combustion temperatures of aerosol (a) mass, (b) ultrafine particle number, and (c) absorption at 422 nm. Missing data indicate that values were below the detection limits of the SMPS (a and b) or the Multi-PAS III (c). Numerical values of the data points are given in SI Table S1. We note that the emission factors should be considered as lower limits due to potential particle losses in the sampling system.

Importantly, the torrefied pine EF_{mass} values are significantly lower than those of raw pine at all temperatures. In concordance with the findings of Maxwell et al.[44], our results suggest that the removal of volatile matter during the torrefaction process (volatile matter content of torrefied pine is 76.40% compared to 85.98% for raw pine; Table 1) plays an important role in limiting aerosol formation in combustion. However, our results contrast with those of previous studies that showed an increase in aerosol emissions for torrefied biomass compared to raw biomass under combustion conditions relevant for power generation[18,43,64]. This could be due to differences in the torrefaction process, but is also likely due to differences in the type of biomass, specifically the ash content. For example, the ash content of the raw and torrefied biomass (corn stalk) in Shao et al.[18] was 8.69% and 11.29%, respectively. In Cheng et al.[43], the ash content of the raw biomass (cotton stalk) was 5.17% and increased to 6.24% - 29.55%, depending on the employed torrefaction process. On the other hand, the ash content of the raw and torrefied pine in our study was 0.27% and 0.35%, respectively. At high combustion temperatures, the carbon in the fuel is converted efficiently to CO_2, and aerosol emissions at these conditions are predominantly inorganic, partly originating from the ash content of the fuel[18]. Therefore, the relatively low ash content of raw and torrefied pine is plausibly the reason for the suppressed EF_{mass} in our high-temperature combustion experiments. This is further evidenced by the trend exhibited by coal combustion. At 400 ºC, EF_{mass} for coal combustion is 3 orders of magnitude lower than raw pine, likely due to the relatively low content of volatile matter (36.58%; Table 1). However, in contrast to the raw and torrefied pine, the coal EF_{mass} increases significantly with increasing temperature and is 3 orders of magnitude higher than raw pine at 800 ºC and 1000 ºC. At these high temperatures, the relatively high inorganic content of coal (6.52% ash and 1.66% sulfur; Table 1) is efficiently oxidized leading to significant inorganic aerosol emissions, as further explored in the chemical speciation subsection.

Figure 2b depicts the number emission factors of ultrafine aerosol particles (EF_{UF}). Ultrafine particles (particles with diameters smaller than 100 nm) induce more severe toxicological effects compared to larger fine particles ($PM_{2.5}$) due to their smaller sizes and larger surface area to volume ratios[65] (Schraufnagel, 2020). Consequently, there are recent efforts to report ultrafine particle emissions from various sources, including domestic burning[34,66]. The trends in EF_{UF} (Figure 2b) are similar to EF_{mass} (Figure 2a) for raw and torrefied pine. Both emission factors exhibit a sharp decrease with increasing combustion temperature, with consistently lower emissions for torrefied pine compared to raw pine. On the other hand, there is a deviation in trends between EF_{mass} and EF_{UF} for coal. Specifically, while the coal EF_{mass} at 1000 °C is 2 orders of magnitude larger than at 400 °C, EF_{UF} is similar at the two temperatures. The reason is that the aerosol size distributions shift to significantly larger sizes with increasing combustion temperature (Supplementary Information (SI) Figure S1). Whereas the aerosol emissions at 400 °C are virtually all ultrafine with a number mode diameter of approximately 20 nm, the emissions at 1000 °C have a number mode diameter of approximately 120 nm with the majority of the mass residing in particles larger than 100 nm. It is also worth noting that while EF_{mass} of raw pine is 3 orders of magnitude higher than coal at 400 °C, EF_{UF} is higher by only one order of magnitude.

Figure 2c depicts the absorption emission factors at 422 nm ($EF_{abs,422}$). Aerosols emitted from the combustion of solid fuels

can contain light-absorbing species, including black carbon (BC) and brown carbon (BrC), which have significant impact on the radiative balance in the atmosphere[62,67]. EF_{abs} represents the total absorption cross-section of the emitted aerosol per unit energy of fuel burned. It depends on both the amount of aerosol as well as its intrinsic light-absorption properties. Therefore, differences in trends between $EF_{abs,422}$ (Figure 2c) and EF_{mass} (Figure 2a) provide insight on differences in aerosol light-absorption properties. For both raw and torrefied pine, $EF_{abs,422}$ decreased with increasing combustion temperature, and there was no measurable absorption at combustion temperatures higher than 600 °C. For raw and torrefied pine, EF_{mass} at 400 °C was larger than at 600 °C by a factor of 17 and 98 respectively. On the other hand, $EF_{abs,422}$ at 400 °C was larger than at 600 °C by a factor of 7 and 21 for raw and torrefied pine, respectively. This indicates that for both fuels, the aerosol produced at 600 °C was intrinsically more light-absorbing. Aerosol emissions from coal combustion exhibited measurable light absorption only at 600 °C and 800 °C. Most significantly, even though coal combustion exhibited high EF_{mass} at 1000 °C, there was no measurable absorption and $EF_{abs,422}$ was effectively zero. As further explored in the subsequent subsections, this indicates a shift in aerosol makeup from carbonaceous species that are light-absorbing (BC and BrC) to inorganic species that exhibit negligible absorption in the visible spectrum.

Light-absorption properties

The imaginary part of the refractive indices at 422 nm (k_{422}) were retrieved from experiments that exhibited measurable absorption at 422 nm and are shown in Figure 3a. At combustion temperature of 400 °C, k_{422} was larger for torrefied pine compared to raw pine. We have previously demonstrated an association between light-absorption properties of carbonaceous aerosols and combustion efficiency[68]. Specifically, higher combustion efficiencies are associated with the production of carbonaceous species that are further along the brown-black continuum[60], and are more light-absorbing. Torrefied pine has a higher carbon content than raw pine (Table 1) and is thus expected to have a higher combustion efficiency, in line with the higher k_{422}.

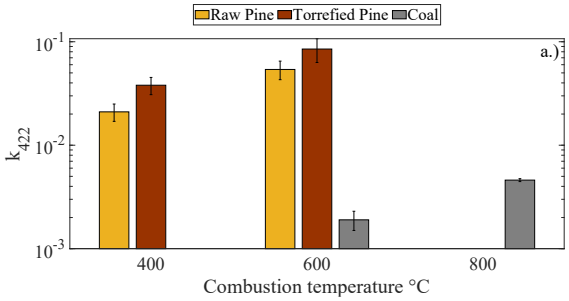

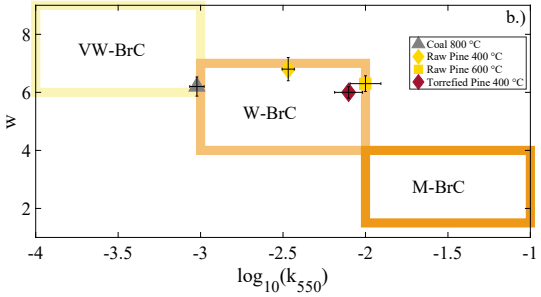

Figure 3. Light-absorption properties of aerosol emissions at different combustion temperatures. Missing values indicate no measurable absorption. (a) Imaginary parts of the refractive indices at 422 nm (k_{422}). (b) Light-absorption properties represented in $\log_{10}(k_{550}) - w$ space. The rectangles represent the BrC categories suggested by Saleh et al.[66] (M-BrC: moderately absorbing BrC; W-BrC: weakly absorbing BrC; VW-BrC: very weakly absorbing BrC). Numerical values of the data points are given in SI Table S2.

For both raw and torrefied pine, k_{422} increased with increasing combustion temperature from 400 °C to 600 °C. This is also in line with our previous findings that everything else held constant, increasing the combustion temperature pushes the carbonaceous aerosol emissions further along the brown-black continuum (i.e. they become more light-absorbing)[60,68]. The dependence of k_{422} on combustion temperature is more nuanced for the coal experiments. It increases with increasing the combustion temperature from 600 °C to 800 °C, but decreases to virtually zero with further increasing the combustion temperature to 1000 °C (there was no measurable absorption at 1000 °C despite the high aerosol emissions). This can be explained by two competing phenomena. On the one hand, the increase in combustion temperature promotes the production of more light-absorbing carbonaceous species. On the other hand, the increase in combustion temperature is also associated with an increase in the production of inorganic species that lower the overall light-absorption efficiency of the aerosol. It is plausible that the first phenomenon was more prominent with temperature increase from 600 °C to 800 °C, while the second phenomenon was dominant with further increase to 1000 °C. We note that at the same combustion temperature of 600 °C, k_{422} of coal aerosol emissions is an order of magnitude smaller than those of raw and torrefied pine emissions, which suggests a significant contribution of inorganic species to the coal emissions.

Four experiments (raw pine at 400 °C and 600 °C, torrefied pine at 400 °C, and coal at 800 °C) had measurable absorption at both 422 nm and 532 nm, which allowed us to calculate w and k_{550} (Equation 2). The results are shown in Figure 3b, with the BrC categories introduced by Saleh[62] shown in the backdrop. All aerosol emissions fall within the weakly-absorbing BrC (W-BrC) category. As mentioned above, we expect that the coal aerosol emissions had a significant inorganic fraction. This does not have a significant effect on the retrieved w, but would potentially push k_{550} to smaller values. Consequently, k_{550} of the BrC fraction of coal emissions is likely larger than the values in Figure 3b, but given the w value of 6.2, the carbonaceous coal emissions are expected to still fall within W-BrC.

Chemical speciation

Offline chemical analyses were performed on the aerosol emissions from 3 experiments: raw pine at 400 ºC, torrefied pine at 400 ºC, and coal at 1000 ºC. We were not able to perform chemical analyses for the other experiments due to the following reasons. The aerosol emissions from raw pine and torrefied pine combustion at temperatures larger than 400 ºC and coal combustion at temperatures less than 800 ºC were too low to enable collecting enough sample within the course of the experiments. And unfortunately, the sample collected from coal combustion at 800 ºC was corrupted during the extraction process. Figure 4 shows the fractions of organic carbon (OC), elemental carbon (EC), and inorganic ions in the aerosol. For both raw and torrefied pine, the emissions at 400 ºC were almost entirely OC, with EC and inorganic ions contributing less than 1% of the aerosol mass. This is expected, because this low combustion temperature is not conducive for producing EC or oxidizing the inorganic content of the fuels. The aerosol emitted from coal combustion at 1000 ºC was predominantly inorganic (85%), with high levels of SO_4^{2-} (65%) and Na^+ (18%) (SI Table S3). OC constituted 15% of the aerosol and there was no EC detected from coal combustion at 1000 °C. This aerosol composition is similar to what is commonly referred to as condensable particulate matter (CPM) in studies of coal-combustion emissions in power generation[50,69,70]. CPM is comprised of inorganic and organic species that are emitted in a gaseous state and condense and form particles as the emissions cool down[28]. We note that the inorganic fraction reported in Figure 4 is likely underestimated, as there are inorganic ions that were not targeted in our IC analysis but could be present in coal emissions (e.g. Ca[69]).

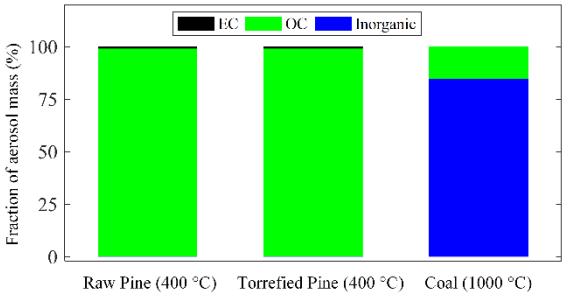

Figure 4. Fractions of EC, OC, and inorganic ions in the aerosol emissions from select experiments. The breakdown of inorganic ions is shown in SI Table S3.

The chemical composition of the organic aerosol fraction of the three samples was further explored using ESI-MS. The number of unique organic compounds identified by MFAssignR was 1773 for raw pine at 400 ºC, 2027 for torrefied pine at 400 ºC, and 182 for coal at 1000 ºC. The small number of identifications for coal is likely due to the particulate emissions being dominated by inorganic ions (Figure 4). Consequently, a significant fraction of organic molecules was probably not present at high enough concentrations in the methanol solution to be efficiently detected by ESI-MS. The diversity in organic molecules in the three samples is illustrated in the van Krevelen diagrams (H:C vs O:C) diagrams in SI Figure S2. As shown in Figure 5a, the organic species detected by ESI-MS were dominated by CHO and CHNO for raw pine and torrefied pine, which is typical for biomass-combustion emissions[71]. Torrefied pine emissions had a smaller fraction of CHO species compared to raw pine (65% vs 79%) and a larger fraction of CHNO species (33% vs 20%). This is possibly due to the torrefaction process leading to lower oxygen content and higher nitrogen content of torrefied pine compared to raw pine (Table 1).

Coal emissions had significant contribution from CHO, CHNO, and CHOS, which is in concordance with previous studies of coal-combustion emissions[39]. The presence of CHOS group in coal emissions supports recent findings that direct emissions from fossil-fuel burning are important contributors to organosulfates in the atmosphere[72]. We also categorized the organic species based on the their modified aromaticity index (AI_{mod})[73,74] into aliphatic ($AI_{mod} = 0$), olefinic ($0 < AI_{mod} \leq 0.5$), and aromatic ($AI_{mod} > 0.5$)[71]. Olefinic compounds were the largest fraction (Figure 5b) and constituted 57%, 53%, and 63% of the molecular formulas for raw pine, torrefied pine, and coal, respectively. Torrefied pine emissions had fewer aromatic species than raw pine (17% vs 22%). Aromatic compounds are precursors for soot formation in combustion[75]. Thus, this result is in agreement with a previous report that torrefaction of biomass reduces the concentration of its sooting components[44]. As shown in Figure S3, the aromatic compounds in raw pine and torrefied pine were more represented in the CHO group, while less than 5% of the molecular formulas in the CHNO group were aromatic. This suggests that nitroaromatic compounds constituted a small fraction of the aromatic species.

To gain insight into the volatility of the organic compounds, we used the parameterization of Li et al.[76] to categorize them into the following volatility bins[77]: intermediate volatility organic compounds (IVOC), semi-volatile organic compounds (SVOC), low-volatility organic compounds (LVOC), and extremely low volatility organic compounds (ELVOC). As shown in Figure 5c, raw pine and torrefied pine emissions exhibited similar volatility distributions. On the other hand, coal emissions had a larger fraction of SVOC, which are expected to be emitted in the gas phase and condense and form particles upon cooling of the emissions. This result further supports our assertion that in this study, coal aerosol emissions at 1000 °C fall under the definition of CPM[28].

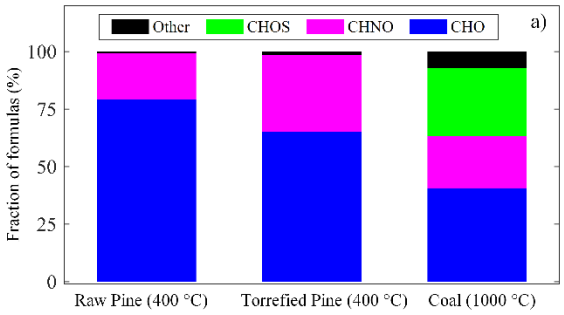

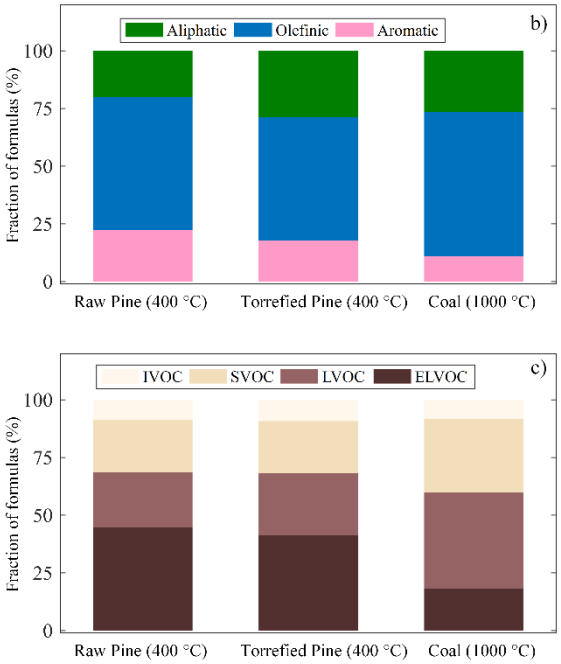

Figure 5. Percentage of molecular formulas of organic aerosol obtained from ESI-MS analysis for select experiments assigned to (a) elemental groups, (b) modified aromaticity index (AI_{mod}) types, and (c) volatility bins.

Conclusion

Our results demonstrate that replacing raw pine with torrefied pine in domestic and power-generation combustion leads to a reduction in particulate emissions, including brown carbon and aromatic species. Furthermore, replacing coal with torrefied pine leads to significant reduction in particulate emissions in power-generation combustion. These results motivate further exploration of emissions from different types of torrefied biomass, their mixtures, as well as co-firing with coal. Overall, our findings support the adoption of torrefied biomass in both domestic and power-generation applications, not only due to its enhanced energy density and reducing greenhouse gas emissions, but also due to reducing particulate pollution. The benefits of reduction in particulate pollution can be monetized and incorporated in techno-economic analyses to provide a more comprehensive assessment of the economic viability of torrefied biomass.

ASSOCIATED CONTENT

Supporting Information

The Supporting Information is available free of charge on the ACS Publications website.

Size distributions of aerosol emissions, van Krevelen plots of organic aerosol, modified aromaticity index types from ESI-MS analysis, aerosol emission factors, aerosol light-absorption properties, fractions of organic carbon / elemental carbon / inorganic ions (pdf).

AUTHOR INFORMATION

Corresponding Author

* Email: rawad@uga.edu. Phone: 706-542-6110

Present Address

† Pacific Northwest National Laboratory, Richland, WA 99352, USA

Funding Sources

Financial support was provided by the National Science foundation Division of Atmospheric and Geospace Sciences (AGS- 2144062) and Division of Chemical, Bioengineering, Environmental, and Transport Systems (CBET-2125064).

ACKNOWLEDGMENT

The authors thank Gregory Vandergrift for his help with MFAssignR and the University of Georgia Proteomics and Mass Spectrometry Core Facility for performing the ESI-MS analysis.

REFERENCES

(1) Anenberg, S. C., Balakrishnan, K., Jetter, J., Masera, O., Mehta, S., Moss, J., and Ramanathan, V. (2013) Cleaner Cooking Solutions to Achieve Health, Climate, and Economic Cobenefits. *Environ. Sci. Technol. 47*, 3944–3952.

(2) Edmund Henrich Eckhard Dinjus, Jörg Sauer, N. D. (2015) The Role of Biomass in a Future World without Fossil Fuels. *Chemie Ing. Tech. 87*.

(3) IEA. (2021) Coal Information: Overview. Paris.

(4) Hannah Ritchie, Max Roser, P. R. (2020) Energy Production and Consumption. *Our World Data*.

(5) Bastakoti, N., Dhital, H. C., and Aryal, A. (2019) Study of Effects of Temperature and Residence Time on Calorific Value of Torrefied Biomass. *Int. J. Eng. Technol. 7*.

(6) Munir, S., Daood, S. S., Nimmo, W., Cunliffe, A. M., and Gibbs, B. M. (2009) Thermal analysis and devolatilization kinetics of cotton stalk, sugar cane bagasse and shea meal under nitrogen and air atmospheres. *Bioresour. Technol. 100*, 1413–1418.

(7) Rijal, B., Gautam, S. H., and LeBel, L. (2020) The impact of forest disturbances on residual biomass supply: A long-term forest level analysis. *J. Clean. Prod. 248*, 119278.

(8) Fisher, E. M., Dupont, C., Darvell, L. I., Commandré, J. M., Saddawi, A., Jones, J. M., Grateau, M., Nocquet, T., and Salvador, S. (2012) Combustion and gasification characteristics of chars from raw and torrefied biomass. *Bioresour. Technol. 119*, 157–165.

(9) Asli Toptas Gozde Duman, Jale Yanik, Y. Y. (2015) Combustion behavior of different kinds of torrefied biomass and their blends with lignite. *Bioresour. Technol. 177*, 328–336.

(10) Ndibe, C., Maier, J., and Scheffknecht, G. (2015) Combustion, cofiring and emissions characteristics of torrefied biomass in a drop tube reactor. *Biomass and Bioenergy 79*, 105–115.

(11) Phanphanich, M., and Mani, S. (2011) Impact of torrefaction on the grindability and fuel characteristics of forest biomass. *Bioresour. Technol. 102*, 1246–1253.

(12) Yuntenwi, E. A. T., MacCarty, N., Still, D., and Ertel, J. (2008) Laboratory study of the effects of moisture content on heat transfer and combustion efficiency of three biomass cook stoves. *Energy Sustain. Dev. 12*, 66–77.

(13) Huangfu, Y., Li, H., Chen, X., Xue, C., Chen, C., and Liu, G. (2014) Effects of moisture content in fuel on thermal performance and emission of biomass semi-gasified cookstove. *Energy Sustain. Dev. 21*, 60–65.

(14) Korus, A., and Szlęk, A. (2015) The effect of biomass moisture content on the IGCC efficiency. *Biomass and Bioenergy 80*, 222–228.

(15) Mani, S., Tabil, L. G., and Sokhansanj, S. (2006) Effects of compressive force, particle size and moisture content on mechanical properties of biomass pellets from grasses. *Biomass and Bioenergy 30*, 648–654.

(16) Sokhansanj, S., Mani, S., Turhollow, A., Kumar, A., Bransby, D., Lynd, L., and Laser, M. (2009) Large-scale production, harvest and logistics of switchgrass (Panicum virgatum L.) – current technology and envisioning a mature technology. *Biofuels, Bioprod. Biorefining 3*, 124–141.

(17) Manouchehrinejad, M., and Mani, S. (2018) Torrefaction after pelletization (TAP): Analysis of torrefied pellet quality and co-products. *Biomass and Bioenergy 118*, 93–104.

(18) Shao, J., Cheng, W., Zhu, Y., Yang, W., Fan, J., Liu, H., Yang, H., and Chen, H. (2019) Effects of Combined Torrefaction and Pelletization on Particulate Matter Emission from Biomass Pellet Combustion. *Energy & Fuels 33*, 8777–8785.

(19) Yue, Y., Singh, H., Singh, B., and Mani, S. (2017) Torrefaction of sorghum biomass to improve fuel properties. *Bioresour. Technol. 232*, 372–379.

(20) van der Stelt, M. J. C., Gerhauser, H., Kiel, J. H. A., and Ptasinski, K. J. (2011) Biomass upgrading by torrefaction for the production of biofuels: A review. *Biomass and Bioenergy 35*, 3748–3762.

(21) M.V. Gil C. Pevida, F. Rubiera, R. G. (2015) Grindability and combustion behavior of coal and torrefied biomass blends. *Bioresour. Technol. 191*, 205–212.

(22) Manouchehrinejad, M., Bilek, E. M. T., and Mani, S. (2021) Techno-economic analysis of integrated torrefaction and pelletization systems to produce torrefied wood pellets. *Renew. Energy 178*, 483–493.

(23) Islam, M. M., Neyestani, S. E., Saleh, R., and Grieshop, A. P. (2022) Quantifying brown carbon light absorption in real-world biofuel combustion emissions. *Aerosol Sci. Technol. 56*, 502–516.

(24) Xie, M., Shen, G., Holder, A. L., Hays, M. D., and Jetter, J. J. (2018) Light absorption of organic carbon emitted from burning wood, charcoal, and kerosene in household cookstoves. *Environ. Pollut. 240*, 60–67.

(25) Simões Amaral, S., Andrade de Carvalho, J., Martins Costa, M. A., and Pinheiro, C. (2016) Particulate Matter Emission Factors for Biomass Combustion. *Atmosphere (Basel). 7*, 141.

(26) Yazdani, A., Dudani, N., Takahama, S., Bertrand, A., Prévôt, A. S. H., El Haddad, I., and Dillner, A. M. (2021) Characterization of primary and aged wood burning and coal combustion organic aerosols in an environmental chamber and its implications for atmospheric aerosols. *Atmos. Chem. Phys. 21*, 10273–10293.

(27) Li, Z., Wang, Y., Lu, Y., and Biswas, P. (2019) Investigation of aerosol and gas emissions from a coal-fired power plant under various operating conditions. *J. Air Waste Manage. Assoc. 69*, 34–46.

(28) Zhang, X., Li, Y., Wang, L., Zhang, Z., and Dong, Y. (2022) Inhibition of coal-fired condensable particulate matter by addition of biomass. *Fuel 310*, 122461.

(29) Chafe, Z. A., Brauer, M., Klimont, Z., Van Dingenen, R., Mehta, S., Rao, S., Riahi, K., Dentener, F., and Smith, K. R. (2014) Household cooking with solid fuels contributes to ambient PM2.5 air pollution and the burden of disease. *Env. Heal. Perspect 122*, 1314–1320.

(30) Lacey Forrest, G., Henze Daven, K., Lee Colin, J., van Donkelaar, A., and Martin Randall, V. (2017) Transient climate and ambient health impacts due to national solid fuel cookstove emissions. *Proc. Natl. Acad. Sci. 114*, 1269–1274.

(31) Joo, H. S., Batmunkh, T., Borlaza, L. J. S., Park, M., Lee, K. Y., Lee, J. Y., Chang, Y. W., and Park, K. (2018) Physicochemical properties and oxidative potential of fine particles produced from coal combustion. *Aerosol Sci. Technol. 52*, 1134–1144.

(32) Mitchell, E. J. S., Lea-Langton, A. R., Jones, J. M., Williams, A., Layden, P., and Johnson, R. (2016) The impact of fuel properties on the emissions from the combustion of biomass and other solid fuels in a fixed bed domestic stove. *Fuel Process. Technol. 142*, 115–123.

(33) Zhang, Y., Schauer, J. J., Zhang, Y., Zeng, L., Wei, Y., Liu, Y., and Shao, M. (2008) Characteristics of Particulate Carbon Emissions from Real-World Chinese Coal

Combustion. *Environ. Sci. Technol. 42*, 5068–5073.

(34) Bilsback, K. R., Dahlke, J., Fedak, K. M., Good, N., Hecobian, A., Herckes, P., L'Orange, C., Mehaffy, J., Sullivan, A., Tryner, J., Van Zyl, L., Walker, E. S., Zhou, Y., Pierce, J. R., Wilson, A., Peel, J. L., and Volckens, J. (2019) A Laboratory Assessment of 120 Air Pollutant Emissions from Biomass and Fossil Fuel Cookstoves. *Environ. Sci. Technol. 53*, 7114–7125.

(35) Rose Eilenberg, S., Bilsback, K. R., Johnson, M., Kodros, J. K., Lipsky, E. M., Naluwagga, A., Fedak, K. M., Benka-Coker, M., Reynolds, B., Peel, J., Clark, M., Shan, M., Sambandam, S., L'Orange, C., Pierce, J. R., Subramanian, R., Volckens, J., and Robinson, A. L. (2018) Field measurements of solid-fuel cookstove emissions from uncontrolled cooking in China, Honduras, Uganda, and India. *Atmos. Environ. 190*, 116–125.

(36) Islam, M. M., Wathore, R., Zerriffi, H., Marshall, J. D., Bailis, R., and Grieshop, A. P. (2021) In-use emissions from biomass and LPG stoves measured during a large, multi-year cookstove intervention study in rural India. *Sci. Total Environ. 758*, 143698.

(37) Weyant, C. L., Chen, P., Vaidya, A., Li, C., Zhang, Q., Thompson, R., Ellis, J., Chen, Y., Kang, S., Shrestha, G. R., Yagnaraman, M., Arineitwe, J., Edwards, R., and Bond, T. C. (2019) Emission Measurements from Traditional Biomass Cookstoves in South Asia and Tibet. *Environ. Sci. Technol. 53*, 3306–3314.

(38) Shen, H., Luo, Z., Xiong, R., Liu, X., Zhang, L., Li, Y., Du, W., Chen, Y., Cheng, H., Shen, G., and Tao, S. (2021) A critical review of pollutant emission factors from fuel combustion in home stoves. *Environ. Int. 157*, 106841.

(39) Song, J., Li, M., Fan, X., Zou, C., Zhu, M., Jiang, B., Yu, Z., Jia, W., Liao, Y., and Peng, P. (2019) Molecular Characterization of Water- and Methanol-Soluble Organic Compounds Emitted from Residential Coal Combustion Using Ultrahigh-Resolution Electrospray Ionization Fourier Transform Ion Cyclotron Resonance Mass Spectrometry. *Environ. Sci. Technol. 53*, 13607–13617.

(40) Weltman, R. M., Edwards, R. D., Fleming, L. T., Yadav, A., Weyant, C. L., Rooney, B., Seinfeld, J. H., Arora, N. K., Bond, T. C., Nizkorodov, S. A., and Smith, K. R. (2021) Emissions Measurements from Household Solid Fuel Use in Haryana, India: Implications for Climate and Health Co-benefits. *Environ. Sci. Technol. 55*, 3201–3209.

(41) Lu, C. M., Dat, N. D., Lien, C. K., Chi, K. H., and Chang, M. B. (2019) Characteristics of Fine Particulate Matter and Polycyclic Aromatic Hydrocarbons Emitted from Coal Combustion Processes. *Energy & Fuels 33*, 10247–10254.

(42) Olugbade, T. O., and Ojo, O. T. (2020) Biomass Torrefaction for the Production of High-Grade Solid Biofuels: a Review. *BioEnergy Res. 13*, 999–1015.

(43) Cheng, W., Shao, J., Zhu, Y., Zhang, W., Jiang, H., Hu, J., Zhang, X., Yang, H., and Chen, H. (2022) Effect of oxidative torrefaction on particulate matter emission from agricultural biomass pellet combustion in comparison with non-oxidative torrefaction. *Renew. Energy 189*, 39–51.

(44) Maxwell, D., Gudka, B. A., Jones, J. M., and Williams, A. (2020) Emissions from the combustion of torrefied and raw biomass fuels in a domestic heating stove. *Fuel Process. Technol. 199*, 106266.

(45) ASTM, D. (2012) D7582–10. Standard Test Methods for Proximate Analysis of Coal and Coke by Macro Thermogravimetric Analysis. *ASTM West Conshohocken, PA, ed*.

(46) ASTM, D. (2015) Standard practice for ultimate analysis of coal and coke. ASTM International.

(47) ASTM, A. (2003) D5865-03–Standard test method for gross calorific value of coal and coke. *Annu. B. ASTM Stand. 5*, 517–527.

(48) Li, Q., Li, X., Jiang, J., Duan, L., Ge, S., Zhang, Q., Deng, J., Wang, S., and Hao, J. (2016) Semi-coke briquettes: towards reducing emissions of primary PM2.5, particulate carbon and carbon monoxide from household coal combustion in China. *Sci. Rep. 6*, 19306.

(49) Magalhaes, D., and Kazanc, F. (2022) Influence of biomass thermal pre-treatment on the particulate matter formation during pulverized co-combustion with lignite coal. *Fuel 308*, 122027.

(50) Feng, Y., Li, Y., Zhang, X., Su, S., Zhang, Z., Gan, Z., and Dong, Y. (2021) Comparative study on the characteristics of condensable particulate matter emitted from three kinds of coal. *Environ. Pollut. 270*, 116267.

(51) Han, J., Yu, D., Yu, X., Liu, F., Wu, J., Zeng, X., Yu, G., and Xu, M. (2019) Effect of the torrefaction on the emission of PM10 from combustion of rice husk and its blends with a lignite. *Proc. Combust. Inst. 37*, 2733–2740.

(52) Molinder, R., and Wiinikka, H. (2015) Feeding small biomass particles at low rates. *Powder Technol. 269*, 240–246.

(53) Xue, X., and Wang, Y. (2013) Particle Size Distribution as a Nonindependent Variable Affecting Pulverized-Coal Burnout in Coal-Fired Power-Plant Boilers. *Energy & Fuels 27*, 4930–4934.

(54) Panahi, A., Tarakcioglu, M., Schiemann, M., Delichatsios, M., and Levendis, Y. A. (2018) On the particle sizing of torrefied biomass for co-firing with pulverized coal. *Combust. Flame 194*, 72–84.

(55) Peng, H., Wang, Y., Wang, Y., Chen, Y., Li, D., and

Xue, H. (2022) Characteristics of emission and light-absorption of size-segregated carbonaceous aerosol emitted from four types of coal combustion at different combustion temperatures. *Atmos. Pollut. Res. 13*, 101265.

(56) Fischer, D. Al, and Smith, G. D. (2018) A portable, four-wavelength, single-cell photoacoustic spectrometer for ambient aerosol absorption. *Aerosol Sci. Technol. 52*, 393–406.

(57) Martinsson, J., Eriksson, A. C., Nielsen, I. E., Malmborg, V. B., Ahlberg, E., Andersen, C., Lindgren, R., Nyström, R., Nordin, E. Z., Brune, W. H., Svenningsson, B., Swietlicki, E., Boman, C., and Pagels, J. H. (2015) Impacts of Combustion Conditions and Photochemical Processing on the Light Absorption of Biomass Combustion Aerosol. *Environ. Sci. Technol. 49*, 14663–14671.

(58) Atwi, K., Mondal, A., Pant, J., Cheng, Z., El Hajj, O., Ijeli, I., Handa, H., and Saleh, R. (2021) Physicochemical properties and cytotoxicity of brown carbon produced under different combustion conditions. *Atmos. Environ. 244*, 117881.

(59) El Hajj, O., Atwi, K., Cheng, Z., Koritzke, A. L., Christianson, M. G., Dewey, N. S., Rotavera, B., and Saleh, R. (2021) Two-stage aerosol formation in low-temperature combustion. *Fuel 304*, 121322.

(60) Saleh, R., Cheng, Z., and Atwi, K. (2018) The Brown–Black Continuum of Light-Absorbing Combustion Aerosols. *Environ. Sci. Technol. Lett. 5*, 508–513.

(61) Saleh, R., Robinson, E. S., Tkacik, D. S., Ahern, A. T., Liu, S., Aiken, A. C., Sullivan, R. C., Presto, A. A., Dubey, M. K., Yokelson, R. J., Donahue, N. M., and Robinson, A. L. (2014) Brownness of organics in aerosols from biomass burning linked to their black carbon content. *Nat. Geosci. 7*.

(62) Saleh, R. (2020) From Measurements to Models: Toward Accurate Representation of Brown Carbon in Climate Calculations. *Curr. Pollut. Reports*.

(63) Cheng, Z., Atwi, K., Hajj, O. El, Ijeli, I., Fischer, D. Al, Smith, G., and Saleh, R. (2021) Discrepancies between brown carbon light-absorption properties retrieved from online and offline measurements. *Aerosol Sci. Technol. 55*, 92–103.

(64) Li, C., Wen, C., Wang, W., Wang, W., Chen, H., Yu, D., and Xu, M. (2019) Reduction effect of co-firing of torrefied straw and bituminous coal on PM1 emission under both air and oxyfuel atmosphere. *Proc. Combust. Inst. 37*, 2723–2731.

(65) Schraufnagel, D. E. (2020) The health effects of ultrafine particles. *Exp. Mol. Med. 52*, 311–317.

(66) Shen, G., Gaddam, C. K., Ebersviller, S. M., Vander Wal, R. L., Williams, C., Faircloth, J. W., Jetter, J. J., and Hays, M. D. (2017) A Laboratory Comparison of Emission Factors, Number Size Distributions, and Morphology of Ultrafine Particles from 11 Different Household Cookstove-Fuel Systems. *Environ. Sci. Technol. 51*, 6522–6532.

(67) Bond, T. C., Doherty, S. J., Fahey, D. W., Forster, P. M., Berntsen, T., DeAngelo, B. J., Flanner, M. G., Ghan, S., Kärcher, B., Koch, D., Kinne, S., Kondo, Y., Quinn, P. K., Sarofim, M. C., Schultz, M. G., Schulz, M., Venkataraman, C., Zhang, H., Zhang, S., Bellouin, N., Guttikunda, S. K., Hopke, P. K., Jacobson, M. Z., Kaiser, J. W., Klimont, Z., Lohmann, U., Schwarz, J. P., Shindell, D., Storelvmo, T., Warren, S. G., and Zender, C. S. (2013) Bounding the role of black carbon in the climate system: A scientific assessment. *J. Geophys. Res. Atmos. 118*, 5380–5552.

(68) Cheng, Z., Atwi, K., Onyima, T., and Saleh, R. (2019) Investigating the dependence of light-absorption properties of combustion carbonaceous aerosols on combustion conditions. *Aerosol Sci. Technol.* 1–16.

(69) Li, J., Qi, Z., Li, M., Wu, D., Zhou, C., Lu, S., Yan, J., and Li, X. (2017) Physical and Chemical Characteristics of Condensable Particulate Matter from an Ultralow-Emission Coal-Fired Power Plant. *Energy & Fuels 31*, 1778–1785.

(70) Wu, Y., Xu, Z., Liu, S., Tang, M., and Lu, S. (2021) Emission characteristics of PM2.5 and components of condensable particulate matter from coal-fired industrial plants. *Sci. Total Environ. 796*, 148782.

(71) Brege, M., Paglione, M., Gilardoni, S., Decesari, S., Facchini, M. C., and Mazzoleni, L. R. (2018) Molecular insights on aging and aqueous-phase processing from ambient biomass burning emissions-influenced Po Valley fog and aerosol. *Atmos. Chem. Phys. 18*, 13197–13214.

(72) Brüggemann, M., Xu, R., Tilgner, A., Kwong, K. C., Mutzel, A., Poon, H. Y., Otto, T., Schaefer, T., Poulain, L., Chan, M. N., and Herrmann, H. (2020) Organosulfates in Ambient Aerosol: State of Knowledge and Future Research Directions on Formation, Abundance, Fate, and Importance. *Environ. Sci. Technol. 54*, 3767–3782.

(73) Koch Dittmar, T., B. P. (2006) From mass to structure: an aromaticity index for high-resolution mass data of natural organic matter. *Rapid Commun. Mass Spectrom. 20*.

(74) B.P. Koch, T. D. (2015) From mass to structure: an aromaticity index for high-resolution mass data of natural organic matter. *Rapid Commun. Mass Spectrom. 30*, 250.

(75) Wang, H. (2011) Formation of nascent soot and other condensed-phase materials in flames. *Proc. Combust. Inst. 33*, 41–67.

(76) Li, Y., Pöschl, U., and Shiraiwa, M. (2016) Molecular corridors and parameterizations of volatility in the chemical evolution of organic aerosols. *Atmos. Chem. Phys. 16*, 3327–3344.

(77) Donahue, N. M., Epstein, S. A., Pandis, S. N., and Robinson, A. L. (2011) A Two-Dimensional Volatility Basis Set : 1 . Organic-Aerosol Mixing Thermodynamics. *Atmos. Chem. Phys. 11*, 3303–3318.

For Table of Contents Only